JOURNAL OF GEOPHYSICAL RESEARCH, VOL. 101, NO. A7, PAGES 15,423–15,432, JULY 1, 1996

Relationship of the ionospheric convection reversal to the hard auroral precipitation boundary

O. A. Troshichev[1] and E. M. Shishkina
Arctic and Antarctic Research Institute, St. Petersburg, Russia

G. Lu and A. D. Richmond
High Altitude Observatory, National Center for Atmospheric Research, Boulder, Colorado

Abstract. Plasma drift and particle measurements from the DMSP spacecraft for the three Geospace Environmental Modeling (GEM) campaign periods (January 27-29, March 28-29, and July 20-21, 1992) have been used to study the relationship between the plasma convection reversal and the poleward boundary of the diffuse auroral zone characterized by hard electron precipitation with energies greater than 0.45 keV. This boundary, named the hard auroral precipitation boundary (or the HAP boundary) in this paper, is often regarded as the ionospheric footprint of the boundary between the central plasma sheet (CPS) and the boundary plasma sheet (BPS). By examining simultaneous ion drift and particle measurements from about 500 satellite passes we find that the large-scale plasma flow in the morning and evening sectors changes its direction within the auroral oval at the HAP boundary. However, exceptions are found in the early morning sector between 0300 and 0600 MLT, where the convection reversal is sometimes (in 30% of the DMSP crossings) displaced poleward relative to the HAP boundary. It is shown that the shape of the region bordered by the HAP boundary can be roughly represented by a circle, whose size is influenced by the IMF B_z component. There is roughly a linear correlation between the diameter of this circle and the cross-polar-cap potential drop, with the best correlation coefficient of 0.65 for winter season. Our study suggests that the HAP boundary corresponds to the magnetospheric boundary between the quasi-dipolar region and the region with more stretched field lines, and the source of the region 1 field-aligned current is located near the HAP boundary. A B_y-dependent shift of the HAP boundary with respect to the noon-midnight meridian is also found. In the northern hemisphere, the shift is dawnward for positive B_y and duskward for negative B_y; in the southern hemisphere, the shift is opposite to that in the northern hemisphere.

1. Introduction

Attempts have been made previously to study the relationship between the auroral oval boundary and the ionospheric convection reversal, and the most common point of view is that the convection reversal occurs somewhere between the trapping boundary of energetic electrons and the poleward boundary of the auroral oval, as identified by the discrete auroral forms [*Heelis et al.*, 1980; *Newell et al.*, 1991; *Nishida et al.*, 1993] Previous studies have been conducted either on statistical bases or through spatially limited observations. The assimilative mapping of ionospheric electrodynamics (AMIE) technique, developed by *Richmond and Kamide* [1988], provides us with global convection patterns in both northern and southern polar regions. These convection patterns are derived by combining a variety of observations, including ground magnetic data from a world-wide network of observatories, and radar and spacecraft measurements of ion drift velocities. The polar-orbiting spacecraft, such as the Defense Meteorological Satellite Program (DMSP) spacecraft, also provide information about the features of auroral precipitating particles. Thus we have a good opportunity to compare auroral boundaries with the structures of ionospheric convection in a global fashion, particularly with the convection reversals. The convection reversal is defined as the locus of points where the convection flow changes its direction from sunward, typically in the auroral oval, to antisunward, typically in the polar cap.

[1]On leave at High Altitude Observatory, National Center for Atmospheric Research, Boulder, Colorado.

Paper number 96JA01192.
0148-0227/96/96JA-01192$09.00

In this paper we shall examine the relationship of the convection reversal and the poleward boundary of the diffuse auroral zone. This boundary separates the diffuse auroral precipitation of hard electrons in the lower-latitude part of the auroral oval from the discrete auroral precipitation of soft electrons in the higher-latitude part of the oval. We thus call it the hard auroral precipitation boundary (hereinafter referred to as the HAP boundary). It should be noted that the HAP boundary is similar but not identical to the transition boundary introduced by *Makita et al.* [1983, 1985]. Although both of them are the boundary between the hard and soft zones of auroral electron precipitation, the transition boundary is defined by where the average energy falls below 0.5 keV [*Makita et al.*, 1983, 1985], whereas the HAP boundary in our analysis uses electron energy of 0.45 keV as a threshold.

2. Method

The separation of the hard and soft zones is difficult in cases when intense spikes of accelerated electrons with energies > 1 keV are observed on the background of soft electron precipitation with energies < 0.5 keV. In such cases the hard electron precipitation is embedded into the regions with soft precipitation and the boundary between the hard and soft zones becomes ambiguous. To overcome this difficulty, we apply the algorithm similar to the one developed by *Troshichev et al.* [1996] to identify the poleward boundary of the oval. We performed a sliding average of particle flux over 1° latitude and define a threshold level as the limit of precipitation in the hard zone. In so doing, we should bear in mind that the intensity of particle fluxes in both hard and soft zones can change considerably from case to case so that a specific flux threshold chosen for one set of conditions might not be appropriate under other conditions. This problem can be solved if the flux values are normalized in some fashion. In our analysis we take the maximum values of electron number flux with energies > 0.45 keV during each ascending and descending portion of the satellite polar pass as an appropriate normalization factor for each oval crossing. Figure 1 shows the typical behavior of this 1°-averaged and normalized electron number flux for the dawn and dusk sectors of the polar region. One can see that electron flux in the auroral oval is much higher than that in the higher-latitude polar region. The boundary between these two regions is generally sharp. As seen in Figure 1, the values of 0.1, 0.15, and 0.20 are practically at the same latitude position. So we choose the value of 0.15 as the threshold level for the identification of the HAP boundary between the diffuse and discrete zones of the auroral oval. Sometimes, during very quiet periods, typically during intervals of northward interplanetary magnetic field (IMF), the intensity of the spikes of accelerated electrons in the central polar region is so large that the averaged fluxes of electrons with energies > 0.45 keV in the polar cap and within the auroral oval turn out to be comparable. In such cases the low-latitude band of the precipitating electrons is considered as the "hard" zone and its poleward edge is correspondingly regarded as the transition boundary. We have examined about 500 DMSP polar crossings in both northern and southern hemispheres. The HAP boundary has been identified in three fourths of these crossings. In the rest of the cases, the spacecraft either did not cross the HAP boundary (i.e., the orbit was at lower latitudes) or the boundary cannot be identified owing to very low level of particle precipitation.

The AMIE procedure is an optimally constrained, weighted least squares fit of coefficients to the observed data. The procedure first modifies statistical conductivity models by incorporating direct and indirect observations of the height-integrated conductances to provide an improved temporal and spatial resolution of high-latitude ionospheric conductivity. Energy fluxes and average energies of the auroral precipitating electrons measured by the polar-orbiting satellites, such as DMSP and TIROS-NOAA spacecraft, are used to calculate the height-integrated Pedersen and Hall conductivities, based on the empirical formulas of *Robinson et al.* [1987]. In addition, the magnetic perturbations measured by ground magnetometers are also used to modify the ionospheric conductivities [*Ahn et al.*, 1983]. Once a reliable conductivity distribution is derived, the ionospheric convection pattern can be estimated from the direct ion drift observations by satellites and radars,

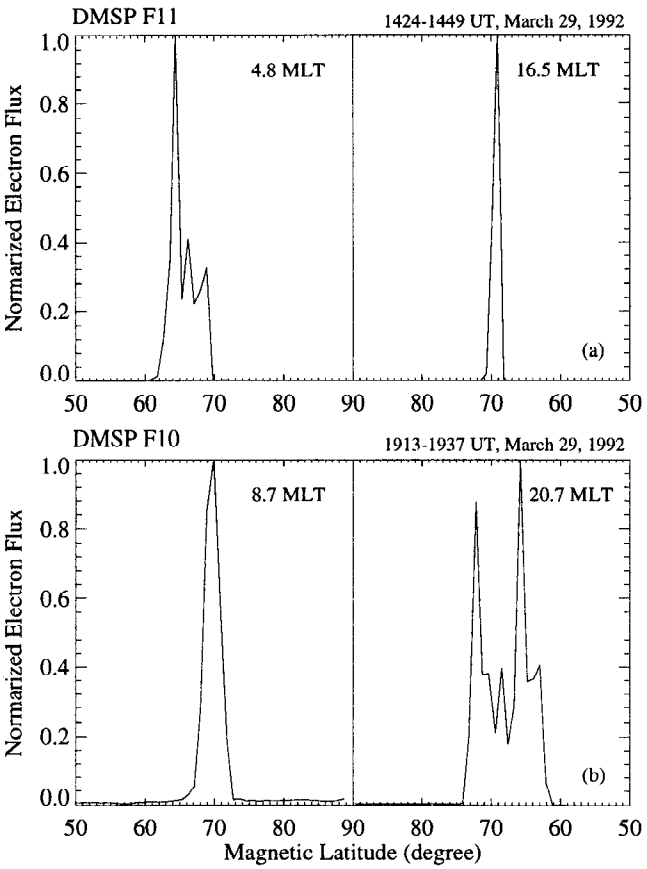

Figure 1. Distributions of normalized electron number flux for the dawn and dusk sectors in the polar region.

and from the inversion of magnetic perturbations. Additionally, an a priori statistical potential model is applied, which provides a first-order estimate of the ionospheric potentials where there are no in situ measurements. The different data sets are weighted by the inverse square of their effective errors so that less reliable data contribute less to the fitting. The detailed fitting procedure has been described by *Richmond and Kamide* [1988] and *Richmond* [1992]. AMIE uses apex coordinates [*VanZandt et al.*, 1972; *Richmond*, 1995], with the apex latitude being similar to the invariant latitude and corrected geomagnetic latitude in high-latitude regions. All data are converted to apex coordinates before being fed into AMIE. The current grid size of AMIE is about 1.7° in latitude and 10° in longitude.

3. Results

Patterns of the high-latitude ionospheric electrodynamic fields are constructed by using the AMIE technique for a total of 7 days from the three Geospace Environmental Modeling (GEM) periods: January 27-29, March 28-29, and July 20-21, 1992. To derive these patterns, we have utilized the satellite ion drift and precipitating particle measurements that are taken within ±15 min of each analyzed time. Radar observations of plasma drift within ±5 min and ground magnetometer data averaged over 5 min in the vicinity of each given time are also used in the AMIE fitting procedure.

Figure 2 shows representative patterns of plasma convection (top row) and field-aligned current (bottom row) for different IMF orientations. Figure 2a shows the typical two-cell convection pattern observed when the IMF is southward, with antisunward convection in the high-latitude polar cap and return sunward convection in lower latitudes in the auroral zone. The two-cell pattern with dawn-dusk asymmetry due to the influence of the IMF azimuthal component is shown in Figure 2c. Figure 2e is a pattern of four cells, with two reversed cells in the central polar region and two weaker and distorted cells at lower latitudes. Such pattern is typical for strongly northward IMF conditions [*Knipp et al.*, 1993; *Lu et al.*, 1994]. The large black dots on these patterns indicate the location identified as the HAP boundary where the normalized electron flux drops below the threshold level of 0.15. One can see that the convection reversal often coincides with the HAP boundary, even under northward IMF conditions. In the case of strongly northward IMF (Figure 2e), the lower-latitude convection reversals, not the high-latitude ones, are located along the HAP boundary. When one of the cells, morning or evening, encompasses almost the whole polar region under the influence of the large IMF y component, velocity shears rather than reversals are often observed at some locations along the HAP boundary (Figure 2c). To distinguish from the flow reversal which separates sunward and antisunward convection, in this paper the velocity shear includes locations where there is a discontinuity in the flow speed but not necessary in the flow direction.

Figure 3 presents the statistical relationship between the convection reversal and the HAP boundary in the morning and evening sectors of the northern and southern polar regions. All events of simultaneous observations of the convection reversal and HAP boundary are divided into five categories: concurrence of the two boundaries within 1 degree; with 1-3 deg of displacement, poleward and equatorward; and with more than 3 deg of poleward and equatorward displacement. The displacement is positive if the convection boundary is equatorward of the HAP boundary; otherwise, it is negative. The solid lines in Figure 3 are for the cases with the convection reversals, and the dashed lines are for those with the velocity shears. One can see that the HAP boundary in the evening sector coincides with either the convection reversal or the velocity shear in an overwhelming majority of cases. Cases with displacements toward pole or equator happen with almost equal probability. In contrast to the evening sector, the HAP boundary in the morning sector coincides with the convection reversal only in 60% of the auroral oval crossings, and there is an apparent equatorward displacement of the HAP boundary with respect to the convection reversal usually in the 0300-0600 MLT sector. It is noteworthy that the concurrence of the HAP boundary and the convection reversal takes place independent of magnetic activity or the sign of the IMF B_z component. The velocity shear in our examination is seen more often in the evening sector, where a round-shaped negative potential cell becomes spatially dominant owing to the B_y effect.

If the location of the HAP boundary is determined by more than three points, we can estimate the shape of the region bordered by the HAP boundary. This region is likely to be circular regardless of the IMF orientation. These circles are also drawn in Figure 2. Thus we conclude that the poleward boundary of the homogeneous hard electron precipitation (i.e., the HAP boundary) forms a circle in the polar region. For simplicity, we call this circle the HAP circle. The large-scale electric fields change their orientation along this HAP circle or somewhat poleward of it in the morning sector.

In spite of small-scale structures of the field-aligned currents, the large-scale distributions (the bottom row in Figure 2) show upward region 1 and downward region 2 currents on the duskside, and downward region 1 and upward region 2 currents on the dawnside, similar to the statistical patterns of *Iijima and Potemra* [1978]. When the IMF B_y is strongly positive (Figure 2d), the afternoonside upward region 1 current expands into the morning side, and overlaps in longitude with the downward region 1 current in the prenoon sector. This most poleward field-aligned current coincides with the mantle precipitation and thus is often referred to as the "mantle current" [*Bythrow et al.*, 1988; *Erlandson et al.*, 1988]. During strongly northward IMF condition (e.g., Figure 2f), there is an extra pair of field-aligned currents in the central polar cap. These are the so-called NBZ currents [e.g., *Iijima et al.*, 1984; *Potemra et al.*, 1984; *Zanetti et al.*, 1984]. By examining the

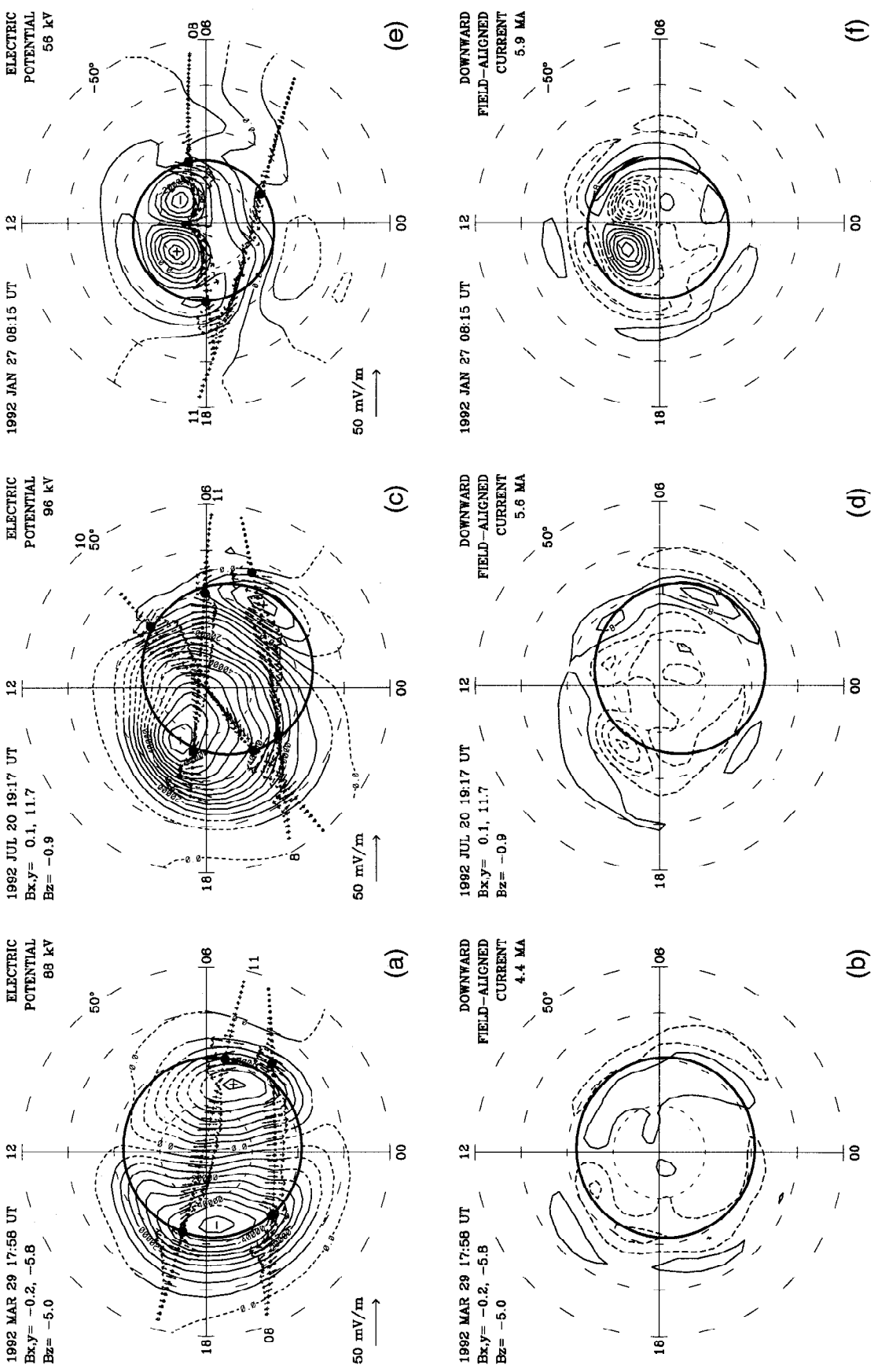
ELECTRIC POTENTIAL 88 kV
1992 MAR 29 17:58 UT
Bx,y= −0.2, −5.8
Bz= −5.0
50 mV/m
(a)
DOWNWARD FIELD−ALIGNED CURRENT 4.4 MA
1992 MAR 29 17:58 UT
Bx,y= −0.2, −5.8
Bz= −5.0
(b)
ELECTRIC POTENTIAL 96 kV
1992 JUL 20 19:17 UT
Bx,y= 0.1, 11.7
Bz= −0.9
50 mV/m
(c)
DOWNWARD FIELD−ALIGNED CURRENT 5.6 MA
1992 JUL 20 19:17 UT
Bx,y= 0.1, 11.7
Bz= −0.9
(d)
ELECTRIC POTENTIAL 56 kV
1992 JAN 27 08:15 UT
50 mV/m
(e)
DOWNWARD FIELD−ALIGNED CURRENT 5.9 MA
1992 JAN 27 08:15 UT
(f)

patterns of field-aligned current, we find that the HAP circle often resides at the center of the region 1 current, except in the morning sector where it is sometimes located at the boundary between the region 1 and region 2 currents.

The diameter of the HAP circle seems to be related to the cross-polar electric potential drop, as determined by the AMIE technique. Figure 4 illustrates the relation between the cross-polar-cap potential drop and the diameter of the HAP circle obtained for the three seasons: local summer, local winter, and equinox, and for all seasons. Satellite passes over the northern polar region in July and over the southern polar region in January are combined under local summer conditions. Similarly, data from both hemispheres are included in the plot for the local winter season. A general trend toward the increase of electric potential with the increase of the diameter of the HAP circle is seen in Figure 4, but the data points are scattered, and the correlation coefficient exceeds 0.50 only in the cases of winter and all season. The difference in techniques of estimating the electric potential and the diameter of the HAP circle seems to be the main reason for the incompatibility of these two parameters: the cross-polar-cap potential drop has been estimated as the potential difference between of the foci of the dominant positive and negative potential (or convection) cells, which are sometimes located poleward of and at different distances from the HAP circle.

During the 7 days under study, the IMF data were available only for half the time. We have carefully examined the AMIE patterns that correspond to relatively stable IMF conditions, in which the signs of the IMF components were unchanged for at least 1 hour prior to the given time. Figure 5 presents the scatterplots of the diameter of the HAP circle versus the IMF B_z for both summer and winter seasons. A higher correlation coefficient (r = -0.75) and proportionality factor of -0.51 deg/nT are found for the summer season. For the winter season, the correlation coefficient is -0.53 and the proportionality factor is -0.33 deg/nT.

The center of the HAP circle is apparently shifted with respect to the noon-midnight meridian when the IMF B_y becomes dominant, as shown in Figure 2c. To illustrate if there is any systematic variation in shift corresponding to the change of the IMF B_y, we plot in Figure 6 the dawn-dusk shift with respect to the noon-midnight meridian versus B_y. A positive value represents a dawnward shift and a negative value a duskward shift. In the northern hemisphere, the shift is duskward for negative B_y, and dawnward for positive B_y for both hemispheres. In the southern hemisphere, the shift is opposite to that in the northern hemisphere. The magnitude of the correlation coefficient is about the same in the two hemispheres, and the proportionality factor is also similar but with opposite signs.

4. Discussion

Similar to the transition boundary of *Makita et al.* [1983, 1985], the HAP boundary introduced in this paper is the boundary that divides the hard and soft zones of auroral electron precipitation. According to *Winningham et al.* [1975], these two zones are connected with the central plasma sheet (CPS) located on the near-Earth quasi-dipolar field lines and with the boundary plasma sheet (BPS) that occupies the region with more stretched field lines, respectively. Statistical surveys by *Heelis et al.* [1980] and *Lassen et al.* [1988] have shown a circular shape of the boundary between the BPS and CPS. Our study, which is based on nearly instantaneous global ionospheric mapping, demonstrates for the first time that a circle is a good approximate form for the HAP boundary (and therefore for the boundary between the BPS and CPS). The poleward boundary of the CPS (i.e., the boundary dividing the discrete aurora from the diffuse aurora) is also associated with the stable trapping boundary of energetic electrons [*Deehr et al.*, 1976; *Valchuk et al.*, 1979; *Lyons and Evans*, 1984; *Weiss et al.*, 1992]. Relying on these results, we can regard the HAP boundary identified by our method as the boundary between the quasi-dipolar field line region, containing the trapped energetic electrons, and the stretched field line region, in which stable trapping becomes impossible. If so, the quasi-circular shape of the HAP boundary at the low altitudes is naturally explained by the appropriate form of the region of quasi-dipolar field lines in the inner magnetosphere. Though the HAP boundary can often be approximated as a circle, we realize that it is not always a perfect fit to all data points. As illustrated in Figures 2a and 2c, while most of the dots are fitted well by the circle, a single dot in the morning sector is outside the circle.

Figure 2. (top) Patterns of ionospheric convection for different interplanetary magnetic field (IMF) orientations. The arrows indicate the convection velocities measured by DMSP along the satellite tracks, but in units of electric field. The potential contours are 5 kV. The contours are shown as solid where the assimilative mapping of ionospheric electrodynamics procedure infers an uncertainty of less than 50% in the large-scale electric field; otherwise the contours are dashed. The total cross-polar-cap potential drop given at the upper right is the difference between the most positive and most negative potentials. The dots indicate the hard auroral precipitation (HAP) boundary identified from the DMSP particle measurements (see text for details). The heavy solid circle represents the HAP boundary. (bottom) Distributions of field-aligned current density, with solid lines representing the downward current and dashed lines the upward current. The contour interval is $0.5\mu A/m^2$, starting at $\pm 0.25\mu A/m^2$. The total downward field-aligned current integrated over the area poleward of 50° latitude is given at the upper right.

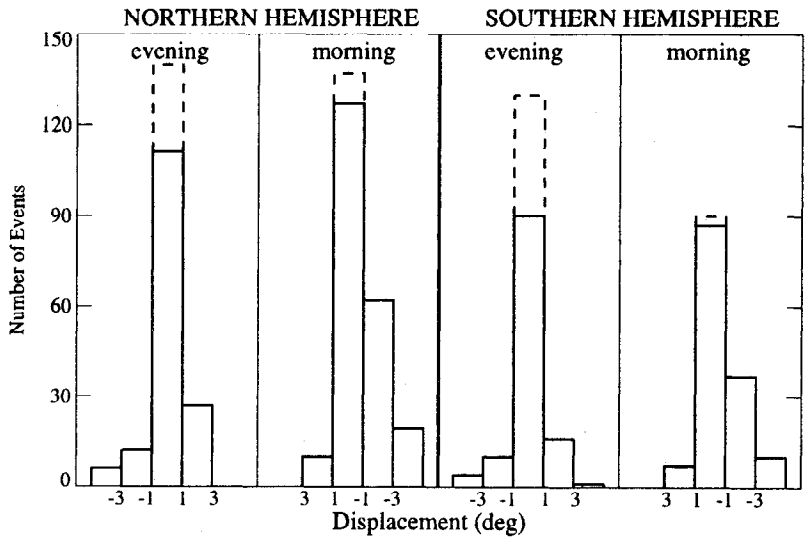

Figure 3. Displacement of the convection reversal with respect to the HAP boundary in the morning and evening sector of the northern and southern polar regions. The displacement is positive if the convection reversal is equatorward of the HAP boundary; otherwise, it is negative. The solid lines are for the cases with convection reversals, and the dashed lines are for the cases with velocity shears.

This is usually true when the IMF B_y becomes large. Nevertheless, the simplified circle still represents well the approximate shape of the HAP boundary, and geometrically it makes things easier to further examine the variations of the HAP boundary in response to the IMF orientations.

General concurrence between the HAP boundary, the convection reversal, and the region 1 field-aligned current implies that the region 1 field-aligned currents also originate along the stable trapping boundary. Previous studies have presented various opinions concerning the location of the region 1 current source: in the part of the plasma sheet closest to its inner edge [*Stern*, 1983]; at the low-latitude boundary layer (LLBL) [*Vasyliunas*, 1979; *Kaufmann et al.*, 1993; *Stasiewicz*, 1991]; in the plasma sheet [*Friis-Christensen and Lassen*, 1991; *Birn*, 1989]; and in the main (central) plasma sheet [*Valchuk et al.*, 1979; *Frank et al.*, 1981; *Ohtani et al.*, 1988]. Since the magnetospheric regions LLBL and BPS are topologically the same [*Vasyliunas*, 1979], it can be considered that the region 1 currents are generated within the BPS region. Our results make it possible to believe that the source of the region 1 currents lies closely to the HAP boundary. Exceptions may take place in the morning sector, where the convection reversal is often displaced by a few degrees toward the pole. Such displacement has been shown in studies by *Heelis et al.* [1980] and *Nishida et al.* [1993] as a common phenomena in the morning hours. Our results show that the poleward displacement of the convection reversal occurs in 30% of the crossings.

The interaction of the solar wind with the magnetosphere directly controls the high-latitude ionospheric electrodynamic features, such as plasma convection and auroral precipitation. As a result, the size of the polar cap as well as the auroral oval varies with the orientation and strength of the IMF, especially the z component of the IMF [*Holzworth and Meng*, 1975; *Meng et al.*, 1977; *Reiff et al.*, 1981; *Wygant et al.*, 1983; *Holzer et al.*, 1986; *Lockwood et al.*, 1990]. On the basis of DMSP auroral images, *Holzworth and Meng* [1984] found that the diameter of the auroral circle increases about 1° with an increase of southward B_z by 1 nT. Our study has also shown a clear dependence of the diameter of the HAP circle on B_z, but the proportionality factor is somewhat smaller, e.g., -0.51 ± 0.10 deg/nT in the summer hemisphere and -0.33 ± 0.09 deg/nT in the winter hemisphere. It is not surprising to see such discrepancy between two independent studies. The auroral circle was defined by *Holzworth and Meng* [1984] as the poleward edge of the auroral oval from DMSP images; whereas in our study the circle represents the auroral HAP boundary determined from the DMSP precipitating particle observations. As discussed above, the HAP boundary is roughly coincident with the poleward boundary of the trapping particles so the HAP boundaries in the two hemispheres should be connected by the same field lines. In other words, the HAP boundary should be on the closed magnetic field lines. Thus one would expect that, in magnetic coordinates, the diameters of the HAP boundaries in the two hemispheres must be the same in order to maintain the total magnetic flux balance. This is consistent with the fact that the average diameter of the HAP circle is about the same in the two hemispheres: 33.6° for the summer hemisphere and 33.5° for the winter hemisphere. Taking into account the statistical uncertainty associated with the fitted parameters, the difference in proportionality factor between the two seasons from our regression fitting should not be considered as significant.

While the z component of the IMF determines the size of the auroral oval, the y component of the IMF

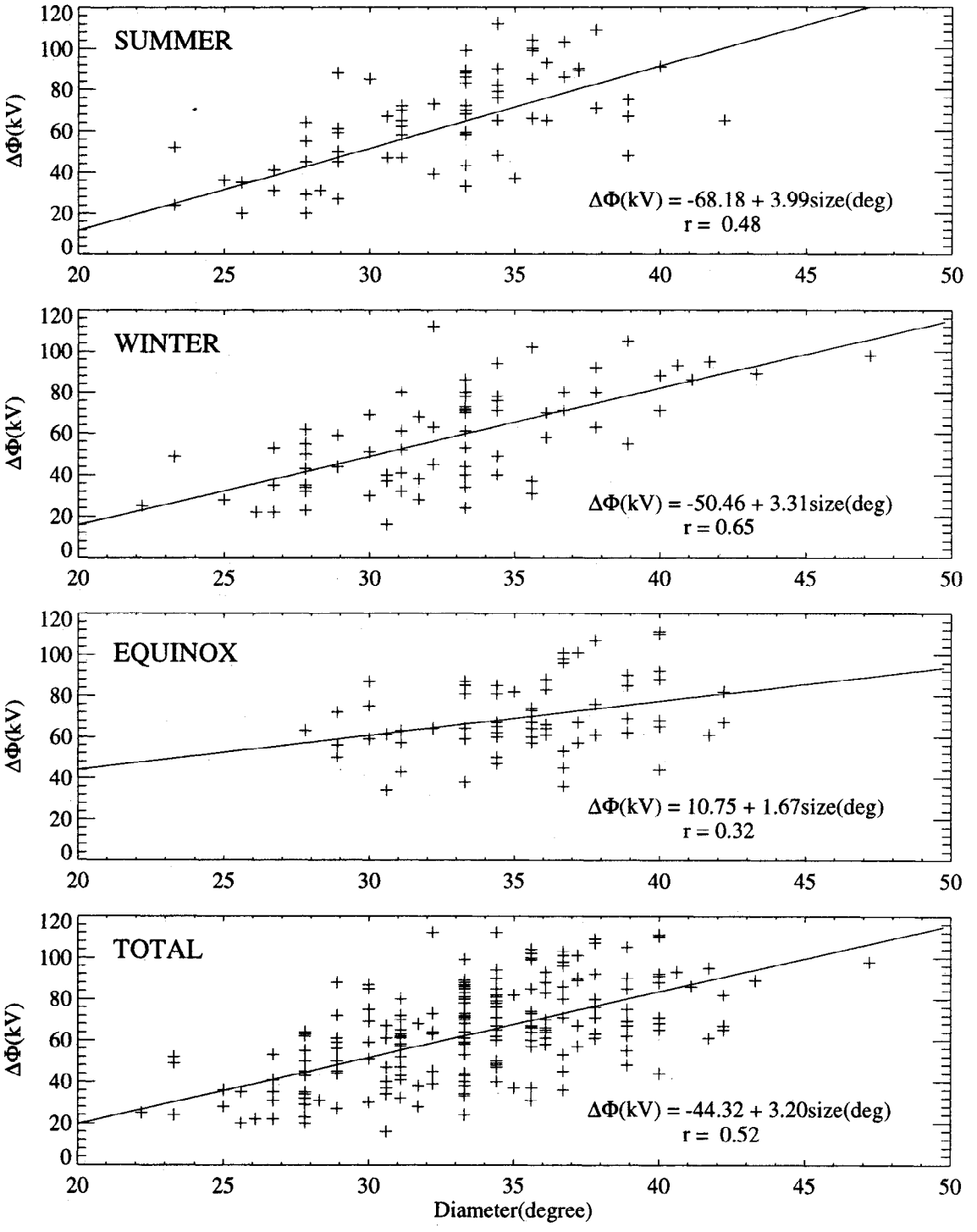

Figure 4. Scatterplots of the cross-polar-cap potential drop versus the diameter of the HAP circle for different seasons. The solid line shows a linear regression fit.

mainly controls the dawn-dusk motion of the oval. A clear trend of the dawn-dusk shift of the auroral oval on the IMF B_y is shown in Figure 6. For positive B_y the auroral oval is shifted toward dawn in the northern hemisphere and toward dusk in the southern hemisphere, and vice versa for negative B_y. A similar tendency was also noted by *Holzworth and Meng* [1984], who found that the center of the auroral circle shifted about 3° duskward in the southern hemisphere when B_y changed from negative to strongly positive. Such dawn-dusk shift of the auroral oval may be attributed to the magnetic tension force due to a large IMF B_y component. Under the influence of the IMF B_y, numerous observations have shown that the dayside ionospheric plas-

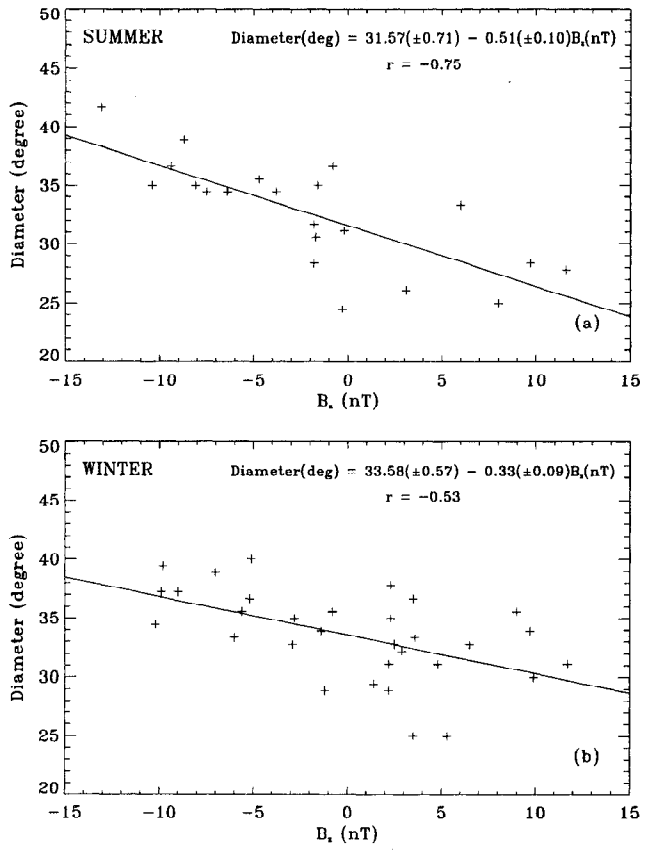

Figure 5. Correlation between the IMF B_z and the diameter of the HAP circle for (top) summer and (bottom) winter seasons.

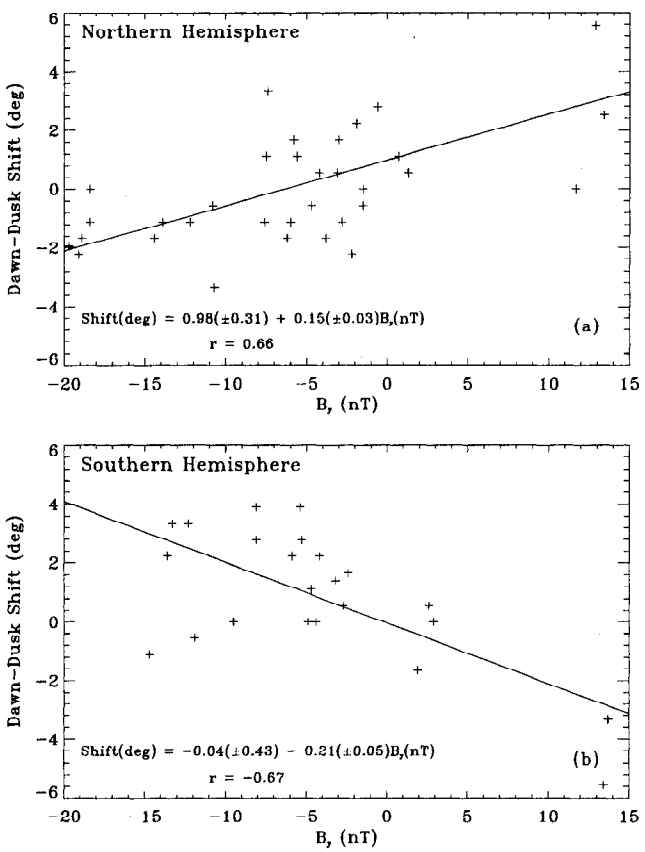

Figure 6. Correlation between the IMF B_y and the dawn-dusk shift of the center of the HAP circle in the (top) northern and (bottom) southern hemispheres.

mas flow dawnward when B_y is positive and duskward when B_y is negative in the northern hemisphere, and vice versa in the southern hemisphere [*Heelis*, 1984; *Reiff and Burch*, 1985; *Heppner and Maynard*, 1987; *Greenwald et al.*, 1990; *Lu et al.*, 1994], which therefore causes open flux tubes to be transported asymmetrically towards dawn or dusk (depending on B_y) [*Xu et al.*, 1995].

5. Conclusions

A specific technique has been applied to identify the HAP boundary that divides the diffuse and discrete auroral electron precipitation. The general form of the HAP boundary is approximately circular in the polar region. The convection reversal and the center of the region 1 current are often found to coincide with this HAP boundary but sometimes lie poleward of it in the morning sector. We thus conclude that the HAP boundary corresponds generally to the boundary between the quasi-dipolar region in the inner magnetosphere and the region with stretched field lines, and the source of the region 1 field-aligned current is located in the vicinity of this boundary. The diameter of the HAP circle is apparently influenced by the IMF B_z. With a southward increase of B_z by 1 nT, the increase of the diameter is about 0.4°. The average diameter of the HAP circle is 33.5°. A reasonably good correlation has also been found between the dawn-dusk shift of the circle center and the IMF B_y. In the northern hemisphere, the center of the HAP circle moves towards dawn (dusk) with $B_y > 0$ ($B_y < 0$). In the southern hemisphere, the HAP circle shifts in the opposite direction to that in the northern hemisphere.

Acknowledgments. We are grateful to B. Emery for valuable comments. The DMSP data were provided by F. Rich and W. Denig. We are indebted to all the participants of the GEM campaigns who have contributed the data used in the AMIE procedure. O. Troshichev would like to thank HAO/NCAR for financial support during his visit. This study was supported in part by NSF under grant 93-SFA.1 and by NASA grants W-17,384 and W-18,536.

The Editor thanks C.-I. Meng and another referee for their assistance in evaluating this paper.

References

Ahn, B. -H., R. M. Robinson, Y. Kamide, and S.-I. Akasofu, Electric conductivities, electric fields and auroral energy injection rate in the auroral ionosphere and their empirical relations to the horizontal magnetic disturbances, *Planet. Space Sci., 31*, 641, 1983.

Birn, J., Three-dimensional equilibria for the extended magnetotail and the generation of field-aligned current sheets, *J. Geophys. Res., 94*, 252, 1989.

Bythrow, P. F., T. A. Potemra, R. E. Erlandson, L. J. Zanetti, and D. M. Klumpar, Birkeland currents and charged particles in the high-latitude prenoon region: A new interpretation, *J. Geophys. Res., 93*, 9791, 1988.

Deehr, C. S., J. D. Winningham, F. Yasuhara, and S.-I. Akasofu, Simultaneous observations of discrete and diffuse auroras by the ISIS-2 satellite and airborne instruments, *J. Geophys. Res., 81*, 5527, 1976.

Erlandson, R. E., L. J. Zanetti, T. A. Potemra, and P. T. Bythrow, IMF B_y dependence of region 1 Birkeland currents near noon, *J. Geophys. Res., 93*, 9804, 1988.

Friis-Christensen, E., and K. Lassen, Large-scale distribution of discrete auroras and field-aligned current, in *Aurora Physics*, edited by C.-I. Meng, M. J. Ryckroft, and L. A. Frank, p. 369, Cambridge Univ. Press, New York, 1991.

Frank, L. A., R. L. McPherron, R. J. DeCoster, B. G. Burek, K. L. Ackerson, and C. T. Russell, Field-aligned currents in the Earth's magnetotail, *J. Geophys. Res., 86*, 687, 1981.

Greenwald, R. A., K. B. Baker, J. M. Ruohoniemi, J. R. Dudeney, M. Pinnrock, N. Mattin, L. M. Leonard, and R. P. Lepping, Simultaneous conjugate observations of dynamic variations in high-latitude dayside convection due to changes in IMF B_y, *J. Geophys. Res., 95*, 8057, 1990.

Heelis, R. A., The effects of interplanetary magnetic field orientation on the dayside high-latitude convection, *J. Geophys. Res., 89*, 2880, 1984.

Heelis, R. A., J. D. Winningham, W. B. Hanson, and J. L. Burch, The relationships between high-latitude convection reversal and the energetic particle morphology observed by Atmosphere Explorer, *J. Geophys. Res., 85*, 3315, 1980.

Heppner, J. P., and N. C. Maynard, Empirical high-latitude electric field models, *J. Geophys. Res., 92*, 4467, 1987.

Holzer, R. E., R. L. McPherron, and D. A. Hardy, A quantitative empirical model of magnetospheric flux transfer process, *J. Geophys. Res., 91*, 3287, 1986.

Holzworth, R. H., and C.-I. Meng, Mathematical representation of the auroral oval, *Geophys. Res. Lett., 2*, 377, 1975.

Holzworth, R. M., and C.-I. Meng, Auroral boundary variations and the interplanetary magnetic field, *Planet. Space Sci., 32*, 25, 1984.

Iijima, T., and T. A. Potemra, Large-scale characteristics of field-aligned currents associated with substorms, *J. Geophys. Res., 83*, 599, 1978.

Iijima, T., T. A. Potemra, L. J. Zanetti, and P. E. Bythrow, Stable patterns of large-scale Birkeland currents in the polar region during strongly northward IMF, *J. Geophys. Res., 89*, 7441, 1984.

Kaufmann, R. L., D. J. Larsson, P. Beidl, and C. Lu, Mapping and energization in the magnctotail, 1, Magnctospheric boundaries, *J. Geophys. Res., 98*, 9307, 1993.

Knipp, D. J., et al., Ionospheric convection response to a magnetic cloud: A case study for 14 January 1988, *J. Geophys. Res., 98*, 18,721, 1993.

Lassen, K., C. Danielsen, and C.-I. Meng, Quiet time average auroral configuration, *Planet. Space Sci., 36*, 791, 1988.

Lockwood, M., S. W. H. Cowley, and M. P. Freeman, The excitation of plasma convection in the high-latitude ionosphere, *J. Geophys. Res., 95*, 7961, 1990.

Lu, G., et al., Interhemispheric asymmetry of the high-latitude ionospheric convection pattern, *J. Geophys. Res., 99*, 6491, 1994.

Lyons, L. R., and D. S. Evans, An association between discrete aurora and energetic particle boundaries, *J. Geophys. Res., 89*, 2395, 1984.

Makita, K., C.-I. Meng, and S.-I. Akasofu, The shift of the auroral electron precipitation boundaries in the dawn-dusk sector in association with geomagnetic activity and interplanetary magnetic field, *J. Geophys. Res., 88*, 7967, 1983.

Makita, K., C.-I. Meng, and S.-I. Akasofu, Temporal and spatial variations of the polar cap dimensions inferred from the precipitation boundaries, *J. Geophys. Res., 90*, 2744, 1985.

Meng, C.-I., R. H. Holzworth, and S.-I. Akasofu, Auroral circle-delineating the poleward boundary of the quiet auroral belt, *J. Geophys. Res., 82*, 164, 1977.

Newell, P. T., W. J. Burke, E. R. Sanchez, C.-I. Meng, M. E. Greenspan, and C. R. Clauer, The low-latitude boundary layer and the boundary plasma sheet at low altitude: Prenoon precipitation regions and convection reversal boundaries, *J. Geophys. Res., 96*, 21,013, 1991.

Nishida, A., T. Mukai, H. Hayakawa, A. Matsuoka, K. Tsuruda, N. Kaya, and H. Fukunishi, Unexpected features of the ion precipitation in the so called cleft/low-latitude boundary layer region: Association with sunward convection and occurrence in open field lines, *J. Geophys. Res., 98*, 11,161, 1993.

Ohtani, S., S. Kokubun, R. C. Elphic, and C. T. Russel, Field-aligned currents in the near-tail region, 1, ISEE observations in the plasma sheet boundary layer, *J. Geophys. Res., 93*, 9709, 1988.

Potemra, T. A., L. J. Zanetti, P. E. Bythrow, A. T. Y. Lui, and T. Iijima, B_y-dependent convection patterns during northward IMF, *J. Geophys. Res., 89*, 9753, 1984.

Reiff, P. H., and J. L. Burch, IMF B_y-dependent plasma flow and Birkeland currents in the dayside magnetosphere, 2, A global model for northward and southward IMF, *J. Geophys. Res., 90*, 1595, 1985.

Reiff, P. H., R. W. Spiro, and T. W. Hill, Dependence of polar cap potential drop on interplanetary parameters, *J. Geophys. Res., 86*, 7639, 1981.

Richmond, A. D., Assimilative mapping of ionospheric electrodynamics, *Adv. Space Res., 12*, 59, 1992.

Richmond, A. D., Ionospheric electrodynamics using magnetic apex coordinates, *J. Geomagn. Geoelectr., 47*, 191, 1995.

Richmond, A. D., and Y. Kamide, Mapping electrodynamic features of the high-latitude ionosphere from localized observations: Technique, *J. Geophys. Res., 93*, 5741, 1988.

Robinson, R. M., R. R. Vondrak, K. Miller, T. Dabbs, and D. Hardy, On calculating ionospheric conductances from the flux and energy of precipitating electrons, *J. Geophys. Res., 92*, 2565, 1987.

Stasiewicz, K., Polar cusp topology and position as a function of interplanetary magnetic field and magnetic activity: Comparison of a model with Viking and other observations, *J. Geophys. Res., 96*, 15,789, 1991.

Stern, D., The origin of Birkeland currents, *Rev. Geophys., 21*, 125, 1983.

Troshichev, O. A., E. M. Shishkina, C.-I. Meng, and P. T. Newell, Identification of the poleward boundary of the auroral oval using characteristics of ion precipitation, *J. Geophys. Res., 101*, 5035, 1996.

Valchuk, T. E., Yu. I. Galperin, J. Crasnier, L. M. Nikolaenko, J. A. Sauvaud, and Y. I. Feldstein, Diffuse auroral zone, IV, Latitudinal distribution of auroral emissions and particle precipitation and its relationship with the plasmasheet and magnetotail (in Russian), *Cosmic Res., 17*, 559, 1979.

VanZandt, T. E., W. L. Clark, and J. M. Warnock, Magnetic apex coordinates: A magnetic coordinate system for the ionospheric F_2 layer, *J. Geophys. Res., 77*, 2406, 1972.

Vasyliunas, V. M., Interactions between the magnetospheric

boundary layers and he ionosphere, in *Proceedings of Magnetospheric Boundary Layers Conference, Eur. Space Agency Spec. Publ.*, SP-148, 1979.

Xu, D., M. G. Kivelson, R. J. Walker, P. T. Newell, and C.-I. Meng, Interplanetary magnetic field control of mantle precipitation and associated field-aligned currents, *J. Geophys. Res., 100*, 1837, 1995.

Weiss, L. A., P. H. Reiff, R. V. Hilmer, J. D. Winningham, and G. Lu, Mapping the auroral oval into the magnetotail using Dynamics Explorer plasma data, *J. Geomagn. Geoelectr., 44*, 1121, 1992.

Winningham, J. D., E. Yasuhara, S.-I. Akasofu, and W. J. Heikkila, The latitudinal morphology of 10-eV to 10-keV electron fluxes during magnetically quiet and disturbed times in the 21.00-03.00 MLT sector, *J. Geophys. Res., 80*, 3148, 1975.

Wygant, J. R., R. B. Torbert, and F. S. Mozer, Comparison of S 3-3 polar cap potential drops with interplanetary magnetic field and models of magnetopause reconnection, *J. Geophys. Res., 88*, 5727, 1983.

Zanetti, L. J., T. A. Potemra, T. Iijima, W. Baumjohann, and P. F. Bythrow, Ionospheric and Birkeland current distributions for Northward interplanetary magnetic field: Inferred polar convection, *J. Geophys. Res., 89*, 7453, 1984.

G. Lu and A. D. Richmond, High Altitude Observatory, National Center for Atmospheric Research, 3450 Mitchell Lane, Boulder, CO 80307.

E. M. Shishkina and O. A. Troshichev, Arctic and Antarctic Research Institute, St. Petersburg, Russia.

(Received October 11, 1995; revised April 1, 1996; accepted April 12, 1996.)